APPLIED SCIENCES AND ENGINEERING

Pascalammetry with operando microbattery probes: Sensing high stress in solid-state batteries

Jonathan M. Larson[1], Eleanor Gillette[2]*, Kristen Burson[1]†, Yilin Wang[1], Sang Bok Lee[2], Janice E. Reutt-Robey[2]‡

Energy storage science calls for techniques to elucidate ion transport over a range of conditions and scales. We introduce a new technique, pascalammetry, in which stress is applied to a solid-state electrochemical device and induced faradaic current transients are measured and analyzed. Stress-step pascalammetry measurements are performed on operando microbattery probes (Li_2O/Li/W) and Si cathodes, revealing stress-assisted Li^+ diffusion. We show how non-Cottrellian lithium diffusional kinetics indicates stress, a prelude to battery degradation. An analytical solution to a diffusion/activation equation describes this stress signature, with spatiotemporal characteristics distinct from Cottrell's classic solution for unstressed systems. These findings create an unprecedented opportunity for quantitative detection of stress in solid-state batteries through the current signature. Generally, pascalammetry offers a powerful new approach to study stress-related phenomena in any solid-state electrochemical system.

INTRODUCTION

Advancements in energy storage research will affect the future of mankind and the environment. While there has been decade-long progress in the development of energy storage solutions for portable electronic devices, major hurdles persist for grid-scale energy storage and for safe vehicular batteries. To address these challenges, the research community is pursuing innovative storage concepts (*1*, *2*), chemistries (*3*–*5*), electrolytes (*6*–*8*), interfacial layerings (*9*–*11*), and geometries (*12*–*14*). To realize these innovations, techniques are needed to characterize charge-transport phenomena over a range of scales and material conditions.

One condition of particular concern in rechargeable batteries is that of stress. High stress within battery systems can naturally arise by electrode swelling/volume change (*15*, *16*), gaseous by-products of side reactions (*17*, *18*), and/or ionic diffusion (*19*, *20*). Stress can eventually lead to performance loss, degradation, and failure. A better physical understanding of ion transport dynamics through stressed battery materials would enable the early sensing of stress and enable effective strategies to mitigate deleterious consequences.

In non-stressed electrochemical systems, ion transport dynamics obey the classic Cottrell equation. This analytical solution of Fick's second law in one dimension provides a convenient expression for diffusion-limited current. The Cottrell equation predicts that diffusion-limited current decays as time$^{-1/2}$ (*21*–*23*) and has been widely confirmed and used. However, as early as 1948, it was reported that this equation would need to be altered for stressed systems (*24*).

In the following decades, rigorous mathematical treatments of stress-assisted diffusion (SAD) were developed (*25*–*28*). SAD is broadly defined here as any physical situation in which stress non-negligibly affects the diffusional behavior of active species within an electrochemical system. In cases of SAD, ion transport dynamics and concentration profiles cannot be adequately described by the conventional Cottrell formalism. Recently, SAD modeling has been extended to energy storage applications (*29*–*32*). While these formulations are fundamentally important and precise, they can include coupling terms, tensors, and/or nonlinear terms and are typically not tractable for most experimental systems.

Nevertheless, possible deviation from Cottrellian behavior due to SAD is intriguing in light of the needs to understand and sense high stress, and its impact on operando energy storage devices. If a specific signal for SAD could be discovered in highly stressed solid electrolytes, then that signal could be used to identify the onset of high levels of stress and, thus, the threat of impending degradation or failure. In the following, we describe the development of pascalammetry, a novel electrochemical/mechanical technique we invented to study stress-related phenomena in electrochemical systems. Here, we also present the first application of pascalammetry used for a controlled study of SAD. In addition, we report a convenient framework for the detection and quantitative analysis of SAD, providing a pathway to sense the onset of high stress in solid-state batteries.

To develop this new pascalammetry technique, we draw direction from voltammetry. In voltammetry, a voltage waveform is applied to an electrochemical system, and induced currents are measured and analyzed (*22*, *23*). In pascalammetry, a stress waveform is applied to an electrochemical system—at constant chemical potential difference (bias voltage)—and induced currents are measured and analyzed. While conventional electrochemistry has been done at various static pressures in the past (*33*), pascalammetry is altogether different, relying on gross dynamic stresses to induce faradaic current responses in electrochemical systems for quantitative analyses.

RESULTS

The electrochemical system used to demonstrate this pascalammetry technique, and study SAD, is a microscopic version of a full-cell, solid-state battery depicted in Fig. 1A. Experiments use a JEOL JSPM-4500A ultrahigh vacuum (UHV), multifunctional scanning probe microscope (SPM), with in situ scanning electron microscope (SEM). The microbattery consists of a microscale half-cell probe (microbattery probe) in contact with an oxide-free silicon (see the Supplementary Materials) electrode (Fig. 1B). For the half-cell probe, a blunted W scanning tunneling microscope (STM) tip functions as a current collector, an ca.

[1]Department of Physics, University of Maryland, College Park, MD 20742, USA.
[2]Department of Chemistry and Biochemistry, University of Maryland, College Park, MD 20742, USA.
*Present Address: Department of Chemistry and Biochemistry, University of San Diego, San Diego, CA 92110, USA.
†Present Address: Department of Physics, Hamilton College, Clinton, NY 13323, USA.
‡Corresponding author. Email: rrobey@umd.edu

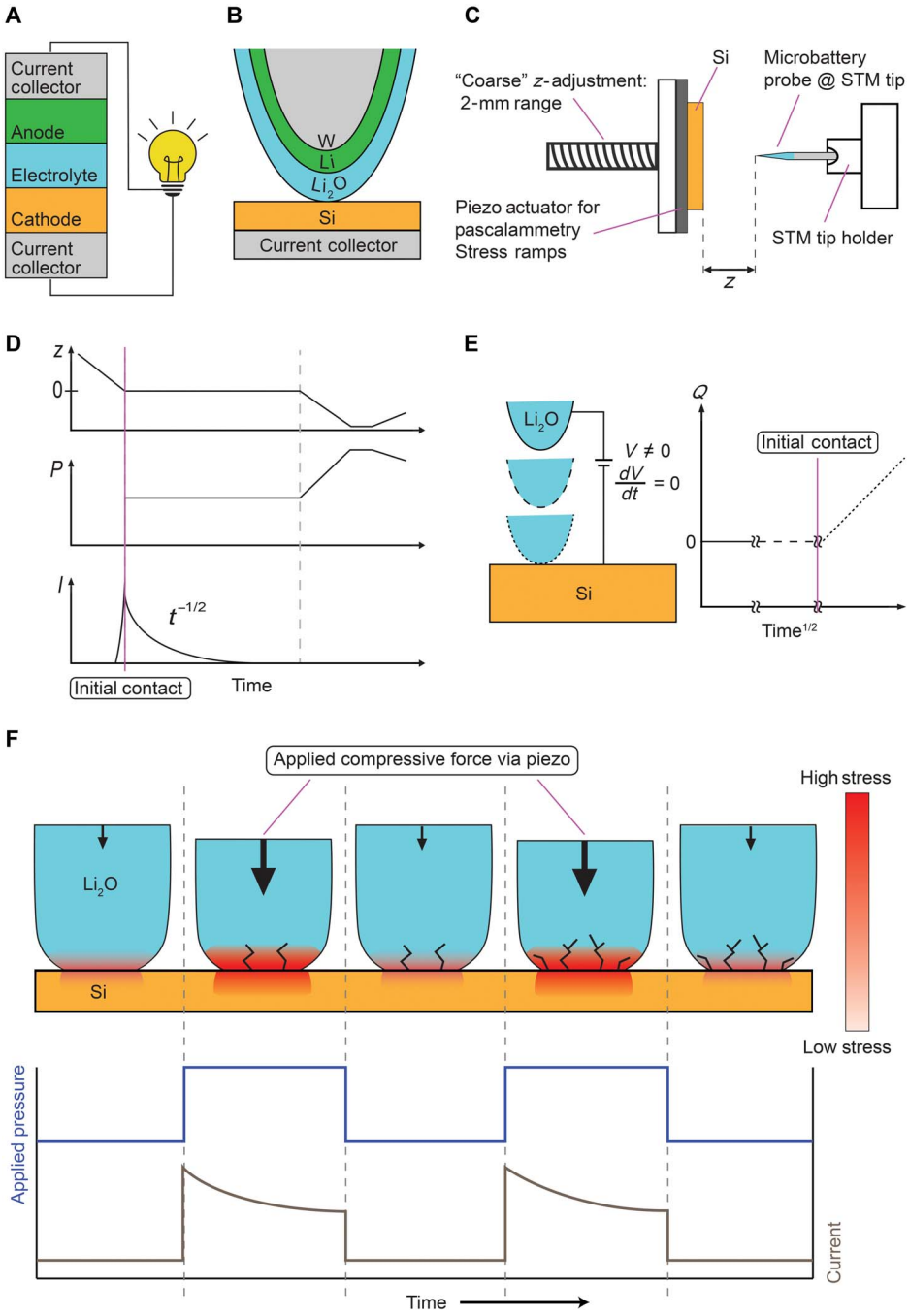

Fig. 1. Scheme for pascalammetry with microbattery probes. (**A**) Cross-sectional schematic of a solid-state battery. (**B**) Cross-sectional schematic of the solid-state microbattery used for pascalammetry measurements. The full cell consists of a microbattery probe in contact with an oxide-free Si cathode. (**C**) Cross-sectional schematic of the scan-probe experimental geometry. The separation distance between the Si cathode and microbattery probe is denoted as *z*. Negative values of *z* correspond to compressive forces/stresses on the full cell. Initial approach is made with a coarse mechanical motor, while compressive forces/stresses are applied via piezo actuator. (**D**) Schematic of signals/protocols used to establish a stable microbattery junction for subsequent pascalammetry measurements. The variables *z*, *P*, and *I* denote separation, applied pressure, and current during approach (left of vertical pink line), initial contact (vertical pink line), validation of diffusion-limited current (current decay obeys Cottrell equation to the right of vertical pink line), and establishment of a more stable junction (right of the vertical dashed gray line). (**E**) Schematic of the biased microbattery probe approaching and contacting the oxide-free Si counter electrode before pascalammetry measurements. Constant bias voltage (V) is applied to promote charging. Solid, dashed, and dotted outlines of the microbattery probe represent different time windows during the approach and after the initial contact with low stress. A corresponding plot of charge versus time$^{1/2}$ is adjacent. The transition from a null signal (solid and dashed) to a linear signal (dotted) indicates an initial contact (pink vertical line) sufficient to establish a full-cell battery and demonstrate diffusion-limited current (time right of the vertical pink line). (**F**) Illustration of microbattery probe/Si cathode junction and signals during two sequential stress-step pascalammetry measurements. In the junction illustration, applied compressive forces (black arrows), stress (clear to red color scale), and mechanical degradation (cracking of the electrolyte coating) are depicted. The pascalammetry signals illustration shows applied stress (pressure) in blue and induced faradaic current transients in gray. Note how this stress-step pascalammetry is analogous to potential-step voltammetry.

10-μm Li metal film coated on the tip functions as the anode, and the ca. 1-μm lithium oxide terminal coating on the Li metal film functions as the solid-state electrolyte. Probe tip geometry and materials are chosen to facilitate pascalammetry measurements on an ideal model system, as described in Materials and Methods.

A full-cell, solid-state microbattery is established using a "coarse" motor to reduce the separation distance "z" between a microbattery probe and a Si(111) cathode until mechanical contact is made (Fig. 1C). During this approach, a constant charging bias condition of −2.0 V Si relative to Li is applied. Mechanical contact is evidenced by a sudden increase in current, at which point the mechanical motor is disengaged, a point called "initial contact" (Fig. 1D). This point of mechanical contact is equivalent to a potential-step voltammetry experiment in that the biased circuit is open until contact is made. The current subsequently decays as time$^{-1/2}$, according to the Cottrell equation, with any capacitive effects disappearing in <0.5 s (see the Supplementary Materials). The microbattery current eventually decays to a steady-state value below our measurement limit (Fig. 1D), indicating that electronic (ionic) contribution to the current signal by leakage and/or tunneling (migration) is negligibly small. All these findings demonstrate measured current upon initial mechanical contact is faradaic and limited by ion diffusion through the minimally stressed lithium oxide electrolyte. Figure 1E provides another graphical representation of the approach and initial contact. The solid, dashed, and dotted outlines of the microbattery represent different times (separation distances) and correspond to the plot of charge Q versus time$^{1/2}$, where Q is the time-integrated current.

After the diffusion-limited faradaic current reaches a steady state, we slowly increase the pressure at constant voltage, such that there is no increase in current or observable morphological change (Fig. 1D time values to the right of the dashed vertical line). This establishes a more stable junction for subsequent measurements. Note that $z < 0$ corresponds to application of compressive forces on the full-cell microbattery and that the microbattery probe with contact area of ca. 2000 μm^2 cannot penetrate the Si cathode. After establishing this stable contact, we proceed with pascalammetry measurements in sets of stress ramps, here called "P-sets." During a given P-set, the chemical potential difference (bias voltage) is kept constant to suppress possible interfacial capacitive charge transfer due to changes in voltage. Figure 1F schematically illustrates a P-set with two successive stress ramps, black arrows represent applied compressive forces, red color gradients represent qualitative stress fields, and the resulting cracks correspond to mechanical degradation.

As described above, once a stable junction is established, pascalammetry experiments are conducted. Figure 2 displays representative data in a top-to-bottom chronological timeline. In situ SEM measurements before/after P-sets are color-coded to match materials in Fig. 1. The gray area in the SEM data is an exposed region of the core W tip, proving a convenient gauge for the thickness of the coating materials. The first SEM image in Fig. 2 is obtained after a minimally stressed stable contact is established and before pascalammetry measurements. Three examples of pascalammetry measurements are presented in Fig. 2 (right side). For clarity, currents are displayed with a third-order Gaussian filter, while all analyses use raw data.

During a stress-step pascalammetry experiment, compressive stresses to the full-cell microbattery are applied with a piezo actuator (see the Supplementary Materials). Stresses to the lithium oxide electrolyte are limited to a maximal value of ca. 800 MPa as described in the Supplementary Materials. All "pressure" signals in Fig. 2 refer to the stress in the electrolyte and are normalized to one, corresponding to the limiting stress value. We find that pascalammetry measurements on our operando device cause current transients attributable to SAD. In addition, mechanical degradation is also evident by comparison of SEM data before and after the pascalammetry measurements. Arrows indicate obvious cracking locations in the middle SEM image. Following multiple stress ramps and retraction of the microbattery probe (bottom SEM), the electrolyte is found to have fractured: Under the bias conditions, the applied stresses (upper bound of ca. 800 MPa) are sufficient to cause mechanical degradation of the lithium oxide electrolyte.

While stress ramps from pascalammetry experiments induce current transients (Fig. 2), it is important to distinguish between faradaic and capacitive effects. Generally, changes in voltage or contact area change the capacitance and induce capacitive charging or discharging. All pascalammetry stress-step measurements are conducted at constant bias voltage to avoid such capacitive charging. We use large contact areas (2000 μm^2) and non-ductile electrolytes so that relative changes in contact area are negligible. Moreover, while capacitance is linearly proportional to contact area, the time constant for capacitive charging/discharging does not depend on the contact area (see the Supplementary Materials). Therefore, if slight contact areal changes occur in sync with a stress step, capacitive charging/discharging contributions to measured current will vanish in less than 0.5 s, as described above and in the Supplementary Materials. We thus confirm that measured stress-induced current transients are faradaic in nature.

DISCUSSION

Analysis of the 27 faradaic current transients arising from stress ramps in pascalammetry measurements confirm that stress can "assist" diffusion and induce currents that cannot be described with the Cottrell equation. In Fig. 3 (A and B), we plot charge versus time (square-root time) for the initial non-stressed contact in black and representative pascalammetry measurement in red. Because the Cottrell equation predicts a functional form for charge versus time to be $Q = at^{1/2}$, plots in Fig. 3 (A and B) are overlaid with appropriate power-law (linear) fits in blue. Initial non-stressed measurements clearly follow the Cottrell equation, whereas the stressed measurements cannot be properly fit with a functional form of $Q = at^{1/2}$. This is emphasized by plotting the power-law fitting parameter γ for all pascalammetry measurements, where the power law is $Q = at^{\gamma}$ (Fig. 3C).

Figure 3C demonstrates that regardless of the sign of the cell voltage (charging or discharging), all SAD faradaic current transients exhibit a similar non-Cottrellian time dependence: $0.5 < \gamma < 1$. This measured range for γ is distinct from a more common deviation from the Cottrell equation (see the Supplementary Materials and fig. S1): diffusion with a driving force, which evolves in a similar manner to a time dependence of $0 < \gamma < 0.5$ as shown in fig. S2. Because of our findings that $0.5 < \gamma < 1$ in all pascalammetry measurements, without exception, we propose this time evolution as a signature for SAD. Next, a concise theory will be presented to describe this time evolution. For convention, $t = 0$ represents the point in time at peak SAD current, just before non-Cottrellian decay begins.

To account for complex stress affects during SAD, we adopt a time-dependent diffusion coefficient and introduce an activation/source term (see the Supplementary Materials), as shown in Eq. 1. We call the resulting approach the "diffusion activation theory" (DAT) for SAD

$$\frac{\partial}{\partial t}C(x,t) = D(t)\nabla^2 C(x,t) + \sum(x,t) \quad (1)$$

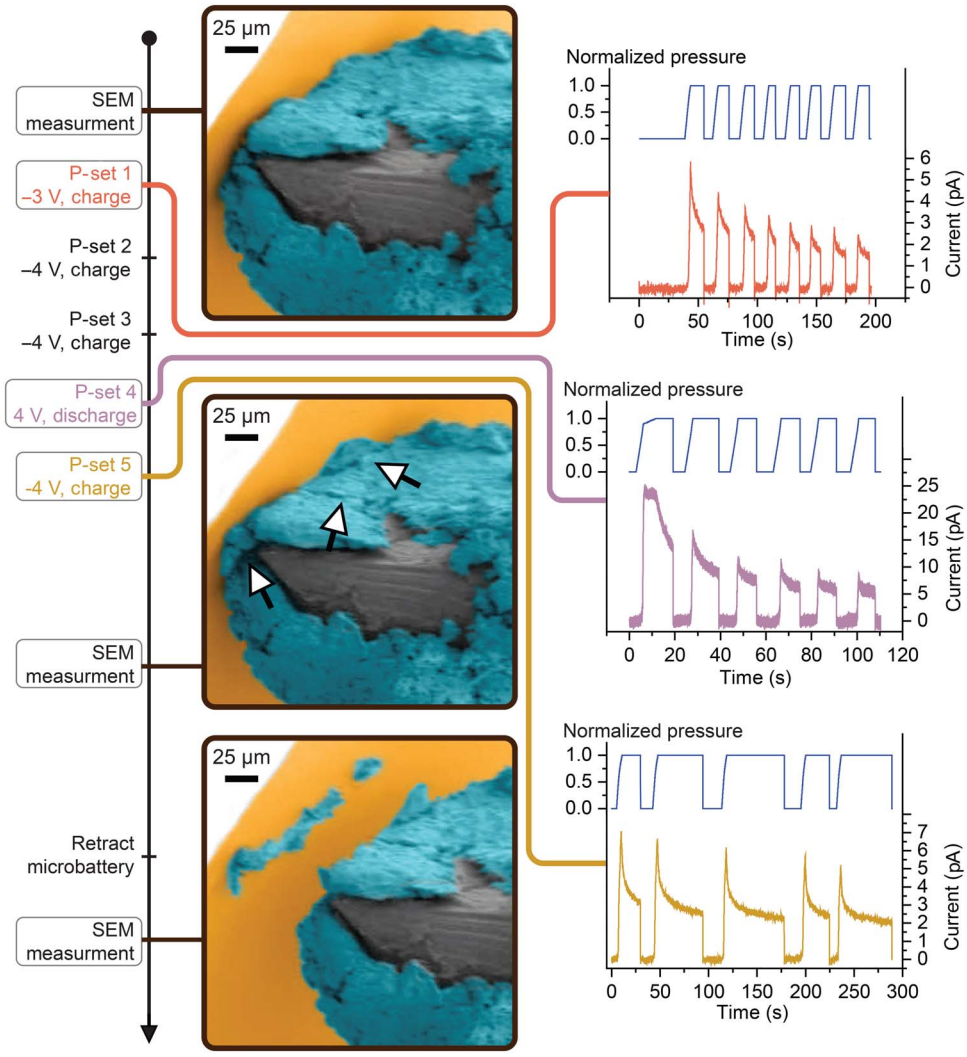

Fig. 2. Pascalammetry and SEM measurement data. Displayed on the left-hand side is a chronology of the experimental measurements that interleave SEM imaging of the junction (center) with pascalammetry measurements (right). Gray boxes on the timeline indicate data shown in this figure. SEM images are color-matched to the material colors in Fig. 1 and show the microbattery probe/Si cathode junction before pascalammetry (top), after pascalammetry (middle), and after retraction of the microbattery probe (bottom). Representative pascalammetry data sets (P-sets) under various constant charging or discharging bias conditions are shown. Each pascalammetry plot traces normalized applied stress/pressure in blue on top and induced faradaic current transients in color on bottom. Current color designates different bias conditions (provided on the time line in corresponding gray boxes). Note that stress-step pascalammetry induces current transients, analogous to potential-step voltammetry. Note also that electrolyte fracture is observed after pascalammetry measurements (middle SEM image), as highlighted with arrows, and pulverization of portions of the microbattery probe is observed after retraction (lower SEM image), consistent with the application of high stresses.

In Eq. 1, $D(t)$ is the stress-assisted, time-dependent diffusion coefficient, and $C(x, t)$ is the concentration of an "active" chemical species (here Li^+) with sufficient energy and a pathway to diffuse. Within this picture, only a fraction of the stoichiometric concentration of a chemical species within a solid electrolyte is active. If energy and/or defects (pathways to diffuse) are added to the electrolyte, through increased stress imparted by an external force or a volumetric expansion of an electrode, then inactive species may be activated. This process cannot be accounted for by a diffusional mechanism and is addressed mathematically by the inclusion of an activation (source) term $\Sigma(x, t)$ in Eq. 1.

We choose $\Sigma(x, t)$ to have linear proportionality, η, to the time derivative of the concentration. This simplification is sometimes used in diffusion problems with local chemical reactions (*34*) and avoids a nonlinear term in the differential equation. The proportionality constant η must range between $0 \leq \eta < 1$. Physically, η represents the time and space averaged percentage of the rate of change in concentration attributable to activation of inactive species. The result in one dimension is a "diffusion/activation equation"

$$\frac{\partial}{\partial t}C(x,t) = \frac{D(t)}{1-\eta}\frac{\partial^2}{\partial x^2}C(x,t) \quad (2)$$

In the following formulation, time "t" has units of seconds, values of one have units of the quantity they are being added to (subtracted from), and the positive constant $u = (1\ \mathrm{s})^{\gamma - 1}$ (see the Supplementary Materials). A general formulation using a dimensionless time variable is also detailed in the Supplementary Materials.

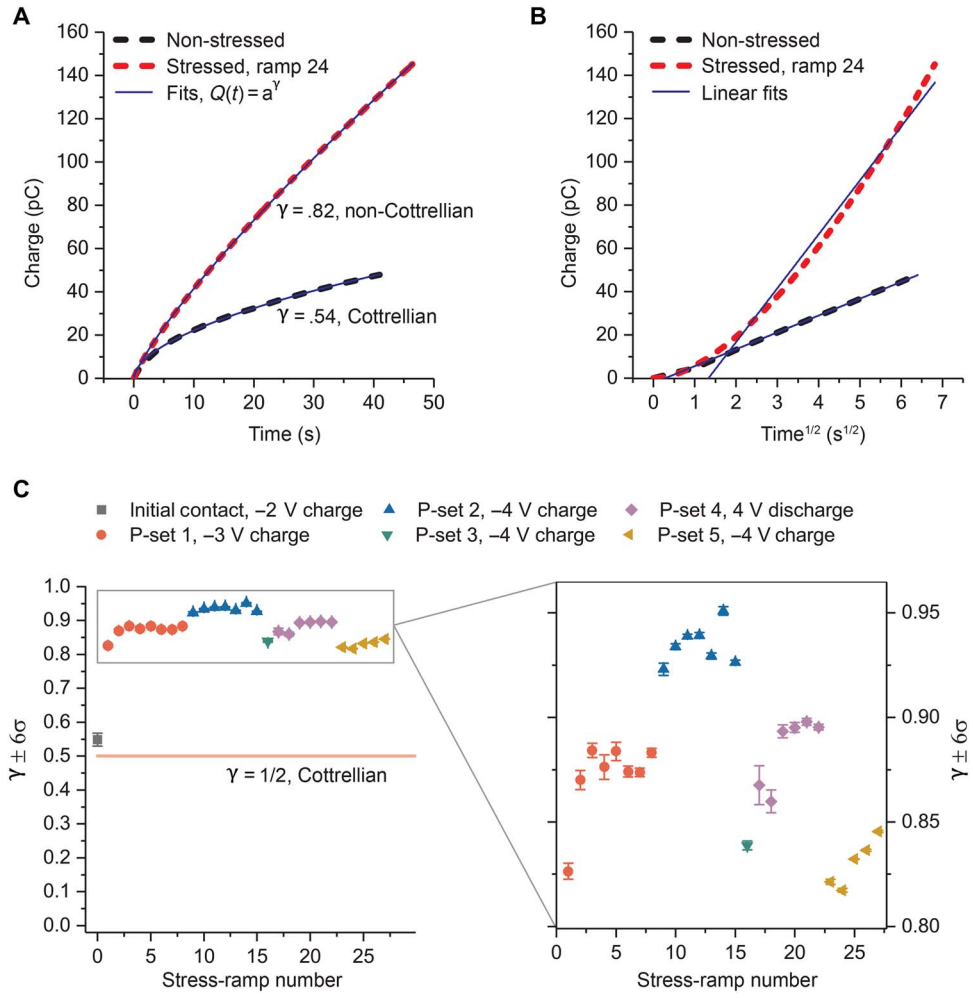

Fig. 3. Faradaic currents in highly stressed microbatteries deviate from Cottrellian behavior and signal SAD. (**A**) Charge (time-integrated current) versus time is plotted for the minimally/non-stressed initial contact (dashed black) and a representative stress-step pascalammetry experiment (dashed red). Power law fitting of form $Q = at^{\gamma}$ (blue traces overlaid) demonstrates that the minimally/non-stressed microbattery follows the time dependence of the Cottrell equation, while the stressed microbattery deviates. (**B**) Plots of the same data from (A) versus time$^{1/2}$, with linear fits overlaid (blue traces). (**C**) Plot of the fitting parameter γ (± 6σ) for non-stressed initial contact (gray) and all pascalammetry measurements (color coded by P-set). Without exception, all stress-step pascalammetry experiments induce current transients that exhibit non-Cottrellian evolution.

The diffusion/activation equation, Eq. 2, is solved (see the Supplementary Materials) over the finite length of the electrolyte and the finite duration of SAD. The analytical solution reads

$$C(x,t) = C^{*}\left(1 + \frac{D_0 k^2[(1+t)^{\gamma} - 1]}{\gamma(1-\eta)u}\right)\frac{\sinh(kx)}{\sinh(kL)} \qquad (3)$$

where L, D_0, C^{*}, and k are the length of the electrolyte, the initial stress-assisted diffusion coefficient, the initial concentration at oxidation interface, and a positive constant, respectively. The parameter η relates to latent species activation as described before. The parameter γ defines the power law of charge evolution and relates physically to stress affects over the time interval being studied. In addition, the time-dependent diffusion coefficient reads

$$D(t) = \frac{D_0(1+t)^{\gamma-1}\gamma(1-\eta)}{D_0 k^2[(1+t)^{\gamma} - 1] + \gamma(1-\eta)u} \qquad (4)$$

which decreases in time. The resulting expression for SAD current, as predicted by the DAT, can thus be written

$$I_{\mathrm{SAD}}(t) = \frac{nFAC^{*}D_0}{\Theta u(t+1)^{1-\gamma}} \qquad (5)$$

In Eq. 5, the structure of $I_{\mathrm{SAD}}(t)$ resembles that of the well-known Cottrell Equation—$nFAC^{*}\sqrt{D}/(\pi t)^{1/2}$ —albeit with non-Cottrellian time dependence. In Eq. 5, F is Faraday's constant, n is the mole number of electrons involved in the interfacial redox reaction, A is the contact area of the reduction interface, and Θ is a positive constant related to L (see the Supplementary Materials) with dimensions of length. Note that no unphysical divergence exists at $t = 0$ s. Equation 5 is as tractable as the Cottrell equation, and fitting charge data from each pascalammetry measurement to the time integral of Eq. 5 demonstrate exceptional agreement between experiment and theory. Plots of the two fitting parameters, with confidence bands of >99.99% (± 6σ), are displayed in Fig. 4A. Also displayed in Fig. 4A is the integral of $I_{\mathrm{SAD}}(t)$,

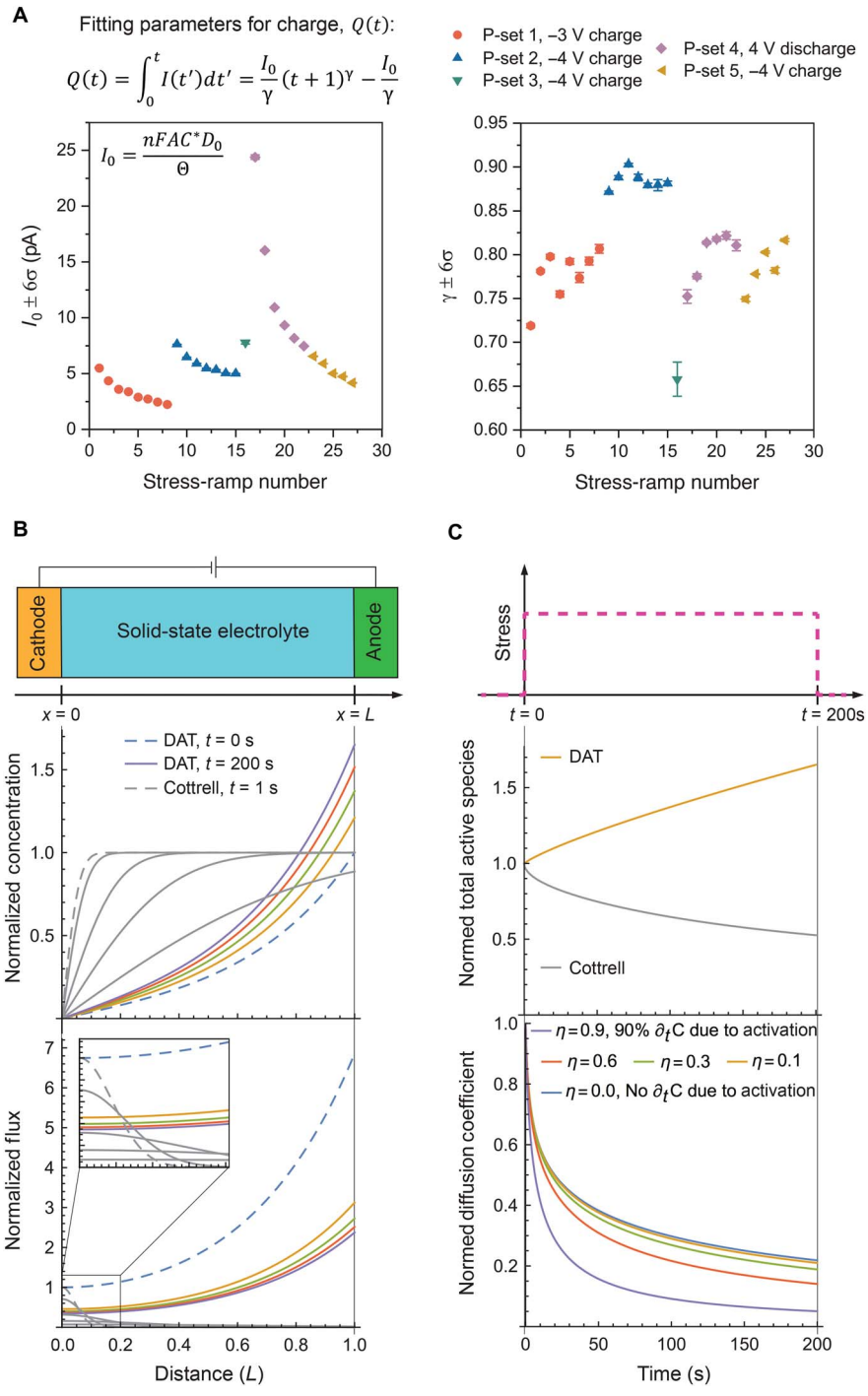

Fig. 4. Analytic solution to a diffusion/activation equation quantifies pascalammetry data, identifies stress-assisted diffusion, and elucidates degradation mechanisms within highly stressed solid-state electrolytes. (**A**) Expression for time-integrated current (charge "*Q*") for the diffusion/activation theory for stress-assisted diffusion, and plots of the fitting parameters for all pascalammetry measurements. $I_0 \pm 6\sigma$ (left hand side) and $\gamma \pm 6\sigma$ (right hand side). (**B**) Plots in this pane share a common horizontal axis corresponding to electrolyte thickness from $x = 0$ to $x = L$. Top: Cross-sectional schematic of an operando solid-state electrochemical storage device. A constant applied potential difference promotes active species to reduce at the cathode/electrolyte interface. Middle: Evolution (0 to 200 s) of active species concentration profiles within the solid-state electrolyte for stress-assisted diffusion/activation (colored) and Cottrellian diffusion (gray). Concentrations are normalized by $C(x, t)/C(L, 0)$, and the early-time curves are dashed. Bottom: Evolution (0 to 200 s) of active species fluxes within the solid-state electrolyte for stress-assisted diffusion/activation (colored) and Cottrellian diffusion (gray). Fluxes are normalized by $j(x, t)/j(0, t_{min})$, and the early-time curves are dashed. (**C**) Plots in this pane share a common horizontal axis of time from $t = 0$ s to $t = 200$ s. Top: Sketch showing the applied stress step of a potential pascalammetry measurement. Middle: Evolution of the normed total active species within the electrolyte [integral of $C(x, t)/C(x, 0)$, from $x = 0$ to $x = L$] for Cottrellian diffusion (gray) and stress-assisted diffusion as described by the diffusion/activation theory (orange). In the diffusion/activation theory for stress-assisted diffusion, the total active species within the electrolyte increases in time. Bottom: Evolution of the normed time-dependent diffusion coefficient, $D(t)/D(0)$, for various fractions of latent species activation.

the charge expression used for fitting, and the fitting parameter $I_0 = I_{SAD}(t = 0)$.

A comparative analysis between the DAT for SAD and Cottrell's solution to Fick's second law is facilitated with Fig. 4 (B and C). Figure 4B displays normalized concentration and flux profiles for SAD (colors) and non-stressed diffusion (gray) over a time interval of 200 s. All plots in Fig. 4B, including the schematic at the top, share the same horizontal axis for electrolyte thickness, and parameters are chosen to match those of our experimental system (*32*). The earliest time plots are dashed, and in the SAD case, concentration increases in time. Notably, a temporal increase in concentration matches the predictions from rigorous continuum and molecular dynamics models of SAD (*30*, *32*). Fluxes are derived from Fick's first law in the usual way. Concentrations are normalized by $C(x, t)/C(L, 0)$, while fluxes are normalized by $j(x, t)/j(0, t_{min})$. For the normalized fluxes, $t_{min} = 0$ s for SAD, while $t_{min} = 1$ s for Cottrell to avoid fictitious divergence.

For the non-stressed Cottrellian case (gray traces in Fig 4B), larger concentrations and fluxes are found at opposite sides of the electrolyte: higher fluxes at the reduction interface and higher concentrations at the oxidation interface. In the case of SAD (colored traces in Fig 4B), described by the DAT, larger concentrations and fluxes both spatially reside at the same interface: the oxidation interface. This has important consequences. The DAT for SAD suggests that SAD itself may contribute to electrolyte degradation near the oxidation interface by mechanical failure due to increased concentration of active species, and/or hot spots, via increased fluxes. While normalized concentrations and fluxes are provided here for purposes of comparative analysis, other plots for the same time interval are also valuable: active species concentration in reference to stoichiometric concentration (fig S3) and active species current density (fig S4).

All plots in Fig. 4C share the same time axis, and the middle and bottom plots are used to visualize important time-dependent physical results of describing SAD with the DAT. The top plot shows a sketch of the applied stress during a pascalammetry measurement, representing a time window in which applied stress crosses a threshold to generate SAD. The middle plot of Fig. 4C is the total active species concentration in the electrolyte as a function of time. Plotted in gold is the prediction that the total active species within an electrolyte increases during SAD. For comparison, the total active species concentration predicted by the Cottrell formalism is also plotted (gray), demonstrating that that formalism cannot replicate a physical phenomenon in which the total amount of active species within the electrolyte is increasing. The bottom of Fig. 4C plots $D(t)/D_0$ for various changes in concentration due to local activation of inactive species. As shown in Eq. 4 and plotted at the bottom of Fig. 4C, the diffusivity decreases in time (as concentration increases) after peak SAD current has been reached at $t = 0$. We note that a decrease in diffusivity in compressively stressed electrochemical systems is also predicated in rigorous continuum and atomistic models (*30*, *31*) within spatial regions of high and increasing concentration. Lastly, from the DAT (*32*), the following inequality is derived

$$J_0 \equiv \frac{I_0}{A} < \frac{nFC^*D_0}{L} \tag{6}$$

which gives an upper bound on the SAD current density, J_0, during a stress step. Because C^* and D_0 both have material-specific realistic ranges, Eq. 6 can be used to estimate electrolyte thicknesses required to suppress or enhance this effect. In this way, scientists and/or engineers desiring to perform pascalammetry, or sense high stresses by the emergence of non-Cottrellian current evolution, can use Eq. 6 as an initial guide for system design.

Generally, pascalammetry is an innovative approach to controllably study all stress-related electrochemical/mechanical phenomena, at any scale. Interesting extensions of the pascalammetry method are numerous, including stress-staircase pascalammetry, linear stress-ramp pascalammetry, and cyclic pascalammetry at varied ramp rates, to name a few. Herein, stress-step pascalammetry is demonstrated for the first time on operando microbattery probes. On the basis of this work, we suggest that scientists and engineers look for ways to monitor operando solid-state batteries for the emergence of stress-assisted diffusional currents evolving according to the derived analog to the Cottrell equation, Eq. 5. The observance of these currents proceeding in time according to $(t + 1)^{\gamma - 1}$, where $0.5 < \gamma < 1$, indicates the presence of elevated stress. Specifically, stress high enough to promote stress-assisted diffusion transients, which include a combination of latent species activation and atypical time-dependent diffusivities and concentrations. This work provides a groundbreaking basis, and opportunity, for sensing and mitigating naturally arising stresses in solid-state batteries.

MATERIALS AND METHODS

Microbattery probe geometry

The microbattery probe geometry and measurement system (JEOL JSPM-4500A) provides a line-of-site side view of the cathode-electrolyte junction edge, a perspective not afforded in typical solid-state coin cells. This perspective was used for intermittent SEM measurements to observe stress-induced morphological changes and degradation, such as cracking. The relatively small cross-sectional area of the active electrolyte facilitated the introduction of large stresses by modest applied compressive forces. This principle has been exploited in a number of works to apply local high pressure with scanning probe tips (*35*).

Microbattery probe materials

In light of the asymmetrical swelling of lithiated Si (*36*), the Si(111) facet was chosen to minimize swelling (*37*). To ensure that lithium oxide was the sole electrolyte in the system, we removed the silicon oxide from the Si cathode by resistive heating in UHV (*38*). The Si(111) surface was heated for ~60 s at 1150°C, quickly cooled to 900°C, and then more slowly cooled to room temperature to reconstruct the Si surface into Si(111)-7 × 7 (*38*). This surface is metallic (*39*) and a good electron and heat conductor, which minimizes Joule and/or stress heating. The ca. 1 mm × 7 mm × 400 μm thick cathode had a surface area that was 3500 times larger than that of the electrolyte, thus serving as both cathode and infinite heat sink. In addition, to suppress possible electron leakage and tunneling currents during pascalammetry experiments, a solid-state electrolyte with a large electron band gap was chosen: Lithium oxide's band gap was reported in the literature to range between 7 and 16 eV (*40*, *41*).

Microbattery probe fabrication

A coating of Li was galvanostatically deposited onto the end of a bluntly cut tungsten STM probe (diameter of 250 μm) via electrodeposition. About 3 mm of the STM tip end is submerged in the aprotic electrolyte, 1 M $LiClO_4$ in propylene carbonate, within an argon glovebox. Lithium metal served as counter electrode, separated from the W tip by a distance of ~2 cm. The galvanostatically controlled current was held at 10 μA for 3 hours, generating films with nominal thicknesses of ~10 μm. Li-coated W tips were stored in argon. Before use, tips were exposed

to atmospheric oxygen for <10 min, generating an ca. 1-μm-thick lithium oxide outer film before being placed under vacuum and transferred into the UHV chamber for measurements.

SUPPLEMENTARY MATERIALS

Supplementary material for this article is available at http://advances.sciencemag.org/cgi/content/full/4/6/eaas8927/DC1

Supplementary Text

Derivation of Eq. 1 in the main text

Derivation of the analytical solution to the diffusion/activation equation in the main text

Derivations of all equations in main text

Derivation of SAD current, main text Eq. 5, and constant Θ

Derivation of max/initial faradaic current density inequality, Eq. 6 in the main text

General formulation of the DAT

Time constant for capacitive charging/discharging

Capacitive time constant is independent of contact area

Applied compressive forces and stresses by piezo actuator

SAD and liquid electrolyte battery systems

Plotting parameters

fig. S1. Current and charge evolution for SAD (experiment), non-stressed diffusion (Cottrell), and diffusion plus a driving force demonstrate distinctness of SAD.

fig. S2. Diffusion plus driving force current evolution and power law with $\gamma < 0.5$, both decay faster than diffusion-limited current (Cottrell).

fig. S3. Temporal evolution of active species concentration within electrolyte during SAD.

fig. S4. Evolution of ionic active species current density within electrolyte during SAD.

Reference (*42*)

REFERENCES AND NOTES

1. B. Huskinson, M. P. Marshak, C. Suh, S. Er, M. R. Gerhardt, C. J. Galvin, X. Chen, A. Aspuru-Guzik, R. G. Gordon, M. J. Aziz, A metal-free organic–inorganic aqueous flow battery. *Nature* **505**, 195–198 (2014).
2. L. Grande, E. Paillard, J. Hassoun, J.-B. Park, Y.-J. Lee, Y.-K. Sun, S. Passerini, B. Scrosati, The lithium/air battery: Still an emerging system or a practical reality? *Adv. Mater.* **27**, 784–800 (2015).
3. J. F. Parker, C. N. Chervin, I. R. Pala, M. Machler, M. F. Burz, J. W. Long, D. R. Rolison, Rechargeable nickel–3D zinc batteries: An energy-dense, safer alternative to lithium-ion. *Science* **356**, 415–418 (2017).
4. H. Wang, Y. Yang, Y. Liang, J. T. Robinson, Y. Li, A. Jackson, Y. Cui, H. Dai, Graphene-wrapped sulfur particles as a rechargeable lithium–sulfur battery cathode material with high capacity and cycling stability. *Nano Lett.* **11**, 2644–2647 (2011).
5. Y. Orikasa, T. Masese, Y. Koyama, T. Mori, M. Hattori, K. Yamamoto, T. Okado, Z.-D. Huang, T. Minato, C. Tassel, J. Kim, Y. Kobayashi, T. Abe, H. Kageyama, Y. Uchimoto, High energy density rechargeable magnesium battery using earth-abundant and non-toxic elements. *Sci. Rep.* **4**, 5622 (2014).
6. L. Suo, O. Borodin, T. Gao, M. Olguin, J. Ho, X. Fan, C. Luo, C. Wang, K. Xu, "Water-in-salt" electrolyte enables high-voltage aqueous lithium-ion chemistries. *Science* **350**, 938–943 (2015).
7. M. Le Thai, G. T. Chandran, R. K. Dutta, X. Li, R. M. Penner, 100k Cycles and beyond: Extraordinary cycle stability for MnO_2 nanowires imparted by a gel electrolyte. *ACS Energy Lett.* **1**, 57–63 (2016).
8. V. Thangadurai, S. Narayanan, D. Pinzaru, Garnet-type solid-state fast Li ion conductors for Li batteries: Critical review. *Chem. Soc. Rev.* **43**, 4714–4727 (2014).
9. K. K. Fu, Y. Gong, B. Liu, Y. Zhu, S. Xu, Y. Yao, W. Luo, C. Wang, S. D. Lacey, J. Dai, Y. Chen, Y. Mo, E. Wachsman, L. Hu, Toward garnet electrolyte-based Li metal batteries: An ultrathin, highly effective, artificial solid-state electrolyte/metallic Li interface. *Sci. Adv.* **3**, e1601659 (2017).
10. X. Han, Y. Gong, K. Fu, X. He, G. T. Hitz, J. Dai, A. Pearse, B. Liu, H. Wang, G. Rubloff, Y. Mo, V. Thangadurai, E. D. Wachsman, L. Hu, Negating interfacial impedance in garnet-based solid-state Li metal batteries. *Nat. Mater.* **16**, 572–579 (2017).
11. J. Zhi, A. Z. Yazdi, G. Valappil, J. Haime, P. Chen, Artificial solid electrolyte interphase for aqueous lithium energy storage systems. *Sci. Adv.* **3**, e1701010 (2017).
12. J. W. Long, B. Dunn, D. R. Rolison, H. S. White, Three-dimensional battery architectures. *Chem. Rev.* **104**, 4463–4492 (2004).
13. A. A. Talin, D. Ruzmetov, A. Kolmakov, K. McKelvey, N. Ware, F. El Gabaly, B. Dunn, H. S. White, Fabrication, testing, and simulation of all-solid-state three-dimensional Li-ion batteries. *ACS Appl. Mater. Interfaces* **8**, 32385–32391 (2016).
14. C. Liu, E. I. Gillette, X. Chen, A. J. Pearse, A. C. Kozen, M. A. Schroeder, K. E. Gregorczyk, S. B. Lee, G. W. Rubloff, An all-in-one nanopore battery array. *Nat. Nanotechnol.* **9**, 1031–1039 (2014).
15. M. Ebner, F. Marone, M. Stampanoni, V. Wood, Visualization and quantification of electrochemical and mechanical degradation in Li ion batteries. *Science* **342**, 716–720 (2013).
16. N. Nitta, F. Wu, J. T. Lee, G. Yushin, Li-ion battery materials: Present and future. *Mater. Today* **18**, 252–264 (2015).
17. J. Vetter, P. Novák, M. R. Wagner, C. Veit, K.-C. Möller, J. O. Besenhard, M. Winter, M. Wohlfahrt-Mehrens, C. Vogler, A. Hammouche, Ageing mechanisms in lithium-ion batteries. *J. Power Sources* **147**, 269–281 (2005).
18. V. Yufit, P. Shearing, R. W. Hamilton, P. D. Lee, M. Wu, N. P. Brandon, Investigation of lithium-ion polymer battery cell failure using x-ray computed tomography. *Electrochem. Commun.* **13**, 608–610 (2011).
19. L. Ji, Z. Guo, Y. Wu, Computational and experimental observation of Li-ion concentration distribution and diffusion-induced stress in porous battery electrodes. *Energy Technol.* **5**, 1702–1711 (2017).
20. J. Zhang, B. Lu, Y. Song, X. Ji, Diffusion induced stress in layered Li-ion battery electrode plates. *J. Power Sources* **209**, 220–227 (2012).
21. F. G. Cottrell, Residual current in galvanic polarization regarded as a diffusion problem. *Z. Phys. Chem.* **42**, 385–431 (1903).
22. A. J. Bard, L. R. Faulkner, *Electrochemical Methods: Fundamentals and Applications*. (Wiley, New York, 2001).
23. R. G. Compton, C. E. Banks, *Understanding Voltammetry*. (World Scientific, 2011).
24. A. H. Cottrell, in *Report of a Conference on Strength of Solids*. (Physical Society, 1948), pp. 30–38.
25. E. C. Aifantis, On the problem of diffusion in solids. *Acta Mech.* **37**, 265–296 (1980).
26. R. Wilson, E. C. Aifantis, On the theory of stress-assisted diffusion, I. *Acta Mech.* **45**, 273–296 (1982).
27. D. J. Unger, E. C. Aifantis, On the theory of stress-assisted diffusion, II. *Acta Mech.* **47**, 117–151 (1983).
28. Y. Weitsman, Stress assisted diffusion in elastic and viscoelastic materials. *J. Mech. Phys. Solids* **35**, 73–93 (1987).
29. A. F. Bower, P. R. Guduru, V. A. Sethuraman, A finite strain model of stress, diffusion, plastic flow, and electrochemical reactions in a lithium-ion half-cell. *J. Mech. Phys. Solids* **59**, 804–828 (2011).
30. H. Haftbaradaran, J. Song, W. A. Curtin, H. Gao, Continuum and atomistic models of strongly coupled diffusion, stress, and solute concentration. *J. Power Sources* **196**, 361–370 (2011).
31. B. Yang, Y.-P. He, J. Irsa, C. A. Lundgren, J. B. Ratchford, Y.-P. Zhao, Effects of composition-dependent modulus, finite concentration and boundary constraint on Li-ion diffusion and stresses in a bilayer Cu-coated Si nano-anode. *J. Power Sources* **204**, 168–176 (2012).
32. Y. Song, X. Shao, Z. Guo, J. Zhang, Role of material properties and mechanical constraint on stress-assisted diffusion in plate electrodes of lithium ion batteries. *J. Phys. D Appl. Phys.* **46**, 105307 (2013).
33. D. Giovanelli, N. S. Lawrence, R. G. Compton, Electrochemistry at high pressures: A review. *Electroanalysis* **16**, 789–810 (2004).
34. J. Crank, *The Mathematics of Diffusion* (Oxford Univ. Press, ed. 2, 1975).
35. C. Lee, X. Wei, J. W. Kysar, J. Hone, Measurement of the elastic properties and intrinsic strength of monolayer graphene. *Science* **321**, 385–388 (2008).
36. X. H. Liu, H. Zheng, L. Zhong, S. Huang, K. Karki, L. Q. Zhang, Y. Liu, A. Kushima, W. T. Liang, J. W. Wang, J. H. Cho, E. Epstein, S. A. Dayeh, S. T. Picraux, T. Zhu, J. Li, J. P. Sullivan, J. Cumings, C. Wang, S. X. Mao, Z. Z. Ye, S. Zhang, J. Y. Huang, Anisotropic swelling and fracture of silicon nanowires during lithiation. *Nano Lett.* **11**, 3312–3318 (2011).
37. X. H. Liu, J. W. Wang, S. Huang, F. Fan, X. Huang, Y. Liu, S. Krylyuk, J. Yoo, S. A. Dayeh, A. V. Davydov, S. X. Mao, S. T. Picraux, S. Zhang, J. Li, T. Zhu, J. Y. Huang, In situ atomic-scale imaging of electrochemical lithiation in silicon. *Nat. Nanotechnol.* **7**, 749–756 (2012).
38. J. M. Larson, S. C. Bharath, W. G. Cullen, J. E. Reutt-Robey, Scanning mwcnt-nanopipette and probe microscopy: Li patterning and transport studies. *Small* **11**, 4946–4958 (2015).
39. K. Oura, V. Lifshits, A. Saranin, A. Zotov, M. Katayama, *Surface Science: An Introduction*. (Springer Science & Business Media, 2013).
40. E. A. Mikajlo, K. L. Nixon, V. A. Coleman, M. J. Ford, The electronic band structure of Li_2O: Testing theoretical predictions using electron momentum spectroscopy. *J. Phys. Condens. Matter* **14**, 3587–3598 (2002).
41. Y. Duan, D. C. Sorescu, Density functional theory studies of the structural, electronic, and phonon properties of Li_2O and Li_2CO_3: Application to CO_2 capture reaction. *Phys. Rev. B* **79**, 014301 (2009).
42. J. Y. Huang, L. Zhong, C. M. Wang, J. P. Sullivan, W. Xu, L. Q. Zhang, S. X. Mao, N. S. Hudak, X. H. Liu, A. Subramanian, H. Fan, L. Qi, A. Kushima, J. Li, In situ observation of the electrochemical lithiation of a single SnO_2 nanowire electrode. *Science* **330**, 1515–1520 (2010).

Acknowledgments: We acknowledge the support of the Maryland NanoCenter and its FabLab. **Funding:** The work was supported by the Nanostructures for Electrical Energy Storage, an Energy Frontier Research Center funded by the U.S. Department of Energy, Office of Science, Office of Basic Energy Sciences under award no. DESC0001160. **Author contributions:** J.M.L., E.G., S.B.L., and J.E.R.-R. developed the initial idea to create probe tips clad with metallic lithium for SPM studies of local lithiation. J.M.L. and E.G. collaborated to fabricate probe tips. J.M.L, K.B., and Y.W. discussed and conducted methods of tip transfer to UHV and prepared and characterized Si cathode substrates. J.M.L. and K.B. conducted initial exploratory SPM and local lithiation experiments. J.M.L. discovered increased pressure on operando microbatteries induced current transients and planned and performed specific SPM experiments to test these effects. J.M.L. conceived of and developed pascalammetry. J.M.L. developed the diffusion/activation theory for stress-assisted diffusion—the analytical framework to quantify pascalammetry data. J.M.L. analyzed all data, generated all figures, and wrote the paper. The paper was then edited and refined by all authors. All authors discussed the results and implications. **Competing interests:** The authors declare that they have no competing interests. **Data and materials availability:** All data needed to evaluate the conclusions in the paper are present in the paper and/or the Supplemental Materials. Additional data related to this paper may be requested from the authors.

Submitted 2 January 2018
Accepted 24 April 2018
Published 8 June 2018
10.1126/sciadv.aas8927

Citation: J. M. Larson, E. Gillette, K. Burson, Y. Wang, S. B. Lee, J. E. Reutt-Robey, Pascalammetry with operando microbattery probes: Sensing high stress in solid-state batteries. *Sci. Adv.* **4**, eaas8927 (2018).